

NANO EXPRESS

Open Access

Comparison of the killing effects between nitrogen-doped and pure TiO₂ on HeLa cells with visible light irradiation

Zheng Li¹, Xiaobo Pan¹, Tianlong Wang¹, Pei-Nan Wang¹, Ji-Yao Chen² and Lan Mi^{1*}

Abstract

The killing effect of nitrogen-doped titanium dioxide (N-TiO₂) nanoparticles on human cervical carcinoma (HeLa) cells by visible light photodynamic therapy (PDT) was higher than that of TiO₂ nanoparticles. To study the mechanism of the killing effect, the reactive oxygen species produced by the visible-light-activated N-TiO₂ and pure-TiO₂ were evaluated and compared. The changes of the cellular parameters, such as the mitochondrial membrane potential (MMP), intracellular Ca²⁺, and nitrogen monoxide (NO) concentrations after PDT were measured and compared for N-TiO₂- and TiO₂-treated HeLa cells. The N-TiO₂ resulted in more loss of MMP and higher increase of Ca²⁺ and NO in HeLa cells than pure TiO₂. The cell morphology changes with time were also examined by a confocal microscope. The cells incubated with N-TiO₂ exhibited serious distortion and membrane breakage at 60 min after the PDT.

Keywords: Nitrogen-doped TiO₂, Visible-light-activated, Photodynamic therapy, Reactive oxygen species

Background

In recent years, semiconductor titanium dioxide (TiO₂) was noticed as a potential photosensitizer in the field of photodynamic therapy (PDT) due to its low toxicity, high stability, excellent biocompatibility, and photoreactivity [1-4]. The electrons in the valence band of TiO₂ can be excited to the conduction band by ultraviolet (UV) radiation with the wavelength shorter than 387 nm (corresponding to 3.2 eV as the band gap energy of anatase TiO₂), thus resulting in the photoinduced hole-electron pairs. These photoinduced electrons and holes can interact with surrounding H₂O or O₂ molecules and generate various reactive oxygen species (ROS, such as superoxide anion radical O₂^{·-} [5], hydroxyl radical OH[·] [6], singlet oxygen ¹O₂ [7], and hydrogen peroxide H₂O₂ [8]), which can react with biological molecules, such as lipids, proteins, and DNA, cause their damages, and eventually kill cancer cells [1,9,10].

However, the pure TiO₂ can only be excited by UV light which is harmful and hinders its practical applications

[11]. Fortunately, recent studies have reported that the optical absorption of TiO₂ in the visible region could be improved by doping [12-14] or dye-adsorbed methods [15,16], which will facilitate the application of TiO₂ as a photosensitizer for PDT. In our previous study [10], we enhanced the visible light absorption of TiO₂ by nitrogen doping and found that the nitrogen-doped TiO₂ (N-TiO₂) showed much higher visible-light-induced photokilling effects on cancer cells than the pure TiO₂.

Although great efforts have been made to prepare doped TiO₂ with visible light absorption, the underlying mechanism of the killing effects of photoactivated TiO₂ on cancer cells has not yet been investigated in details. It is unclear how the TiO₂ interacts with the cancer cells, and what are the differences for their photokilling effects between pure and doped TiO₂. For possible medical applications of N-TiO₂, it is of crucial importance to understand the killing effect of N-TiO₂ on cancer cells and the mechanism of cell damages induced by PDT.

As ROS has been claimed to be of major importance for various kinds of PDT [17-20], the time-dependent ROS productions during visible light irradiation were evaluated in this work for both N-TiO₂ and TiO₂ in aqueous suspensions. The productions of different ROS species, such as O₂^{·-}, H₂O₂, and OH[·], were also studied.

* Correspondence: lanmi@fudan.edu.cn

¹Key Laboratory of Micro and Nano Photonic Structures (Ministry of Education), Department of Optical Science and Engineering, Shanghai Ultra-Precision Optical Manufacturing Engineering Center, Fudan University, 220 Handan Road, Shanghai 200433, China

Full list of author information is available at the end of the article

Furthermore, a systematic comparison of the intracellular parameters with N-TiO₂ and TiO₂ nanoparticles as photosensitizers for PDT was investigated. The changes of mitochondrial membrane potential (MMP), intracellular Ca²⁺, and nitrogen monoxide (NO) concentrations with time after the PDT were measured. The relationships between these parameters were discussed. The morphological changes of cytoskeletons after irradiation were also examined by a confocal microscope at different times after the PDT. The killing effects between pure and nitrogen-doped TiO₂ were compared.

Methods

Preparation and characterization of N-TiO₂ samples

The details of preparation of N-TiO₂ nanoparticles were described in our previous paper [10]. Briefly, The anatase TiO₂ nanoparticles (particle size <25 nm; Sigma-Aldrich, St. Louis, MO, USA) were calcined at a flow rate of 3.5 L/min in ammonia atmosphere at 550°C for 20 min to produce the N-TiO₂ nanoparticles. The crystalline phases of the N-TiO₂ nanoparticles were determined by Raman spectra to be anatase. The ultraviolet-visible (UV/Vis) diffuse reflectance absorption spectra (Additional file 1: Figure S1) of the N-TiO₂ and TiO₂ samples were measured with a Jasco V550 UV/Vis spectrophotometer (Jasco, Inc., Tokyo, Japan).

Pure and N-doped TiO₂ nanoparticles were autoclaved and dispersed in DMEM-H medium at a concentration of 100 μg/ml, respectively. The samples were ultrasonicated for 15 min before using.

Cell culture and PDT treatment

The human cervical carcinoma cells (HeLa) procured from the Cell Bank of Shanghai Science Academy were grown in Petri dishes in DMEM-H solution supplemented with 10% fetal calf serum in a fully humidified incubator at 37°C with 5% CO₂ for 24 h.

The cells were incubated with 100 μg/ml pure or N-doped TiO₂ under light-free conditions for 2 h and were then illuminated with a visible light filtered by a band-pass filter (400 to 440 nm) from a Xe lamp (100-W; Olympus, Center Valley, PA, USA) at a power density of 40 mW/cm² for 5 min. The transmission spectrum of that bandpass filter was shown in Additional file 2: Figure S2. As shown in the figure, the filter could transmit some light with the wavelength below 400 nm. Therefore, the pure TiO₂ could still absorb a small amount of the transmitted light.

Measurement of ROS induced by TiO₂ or N-TiO₂ in aqueous suspensions

For the measurement of photo-induced ROS in TiO₂ or N-TiO₂ aqueous suspensions, 2',7'-dichlorofluorescein (DCFH), was used as a probe. The DCFH was converted

from the diacetate form DCFH (DCFH-DA) (Sigma-Aldrich) by adding 0.5 ml of 1 mM DCFH-DA in methanol into 2 ml of 0.01 N NaOH and keeping the mixture at room temperature in the dark for 30 min. It was then neutralized with 10 ml sodium phosphate buffer (pH = 7.2) [21]. Pure or N-doped TiO₂ in phosphate buffered saline (PBS, 100 μg/ml) were mixed with DCFH (25 μM) before visible light irradiation. The non-fluorescent DCFH can rapidly react with ROS to form fluorescent 2',7'-dichlorofluorescein (DCF). By measuring the fluorescent intensity, the production of ROS could be estimated.

To measure the generations of specific ROS, two probes were used respectively. Dihydrorhodamine 123 (DHR) is mainly sensitive to O₂⁻ [22] and H₂O₂ [23], and 2-[6-(4-aminophenoxy)-3-oxo-3H-xanthan-9-yl]-benzoic acid (APF) is selectively sensitive to OH· [23]. It was already demonstrated that the reactive species H₂O₂, O₂⁻, and ¹O₂ did not cause any modification in the fluorescence of the probe APF [24]. Pure or N-doped TiO₂ in PBS (100 μg/ml) were mixed with DHR (25 μM, Sigma-Aldrich) or APF (10 μM, Cayman Chemical, Ann Arbor, MI, USA) before irradiation. Upon oxidation, the non-fluorescent DHR or APF is converted to the highly fluorescent Rhodamine 123 or fluorescein.

After the samples were irradiated by a visible light (400 to 440 nm) with a power density of 40 mW/cm² for different times ranging from 1 to 5 min, the fluorescence spectra were recorded by a spectrometer (F-2500, Hitachi, Brisbane, CA, USA) and the fluorescent intensities were compared.

MMP assay

Rhodamine 123 [2-(6-amino-3-imino-3H-xanthan-9-yl) benzoic acid methyl ester] (Beyotime, Jiangsu, China), which could bind specifically to the mitochondria, was used to estimate the MMP. When MMP is decreased, the dye could be released from the mitochondria and the fluorescence vanished. The PDT-treated cells were incubated with Rhodamine 123 (5 μg/ml) for 30 min in the dark at 37°C and then were washed with Dulbecco's PBS (D-PBS) for three times before the visible light illumination.

Measurement of Ca²⁺ concentration

To study the intracellular calcium concentration, HeLa cells were loaded with 10 μM Fluo-3 AM (Beyotime) for 30 min at 37°C and followed by washing with D-PBS for three times. Then the cells were incubated for another 20 min to ensure complete cleavage of Fluo-3 AM by the intracellular ester enzyme that releases Fluo-3 before the illumination.

Measurement of intracellular NO

The intracellular NO level was detected using a NO-sensitive fluorescence probe DAF-FM DA [3-amino, 4-

aminomethyl-2',7'-difluorescein, diacetate] (Beyotime). The cells were loaded with 10 μM DAF-FM DA at 37°C in the kit buffer for 20 min and were then gently washed with D-PBS for three times and incubated for another 20 min to ensure that the intracellular DAF-FM DA was completely catalyzed to form DAF-FM by ester enzyme before the illumination.

Cell morphology and cytoskeleton observation

The HeLa cells were fixed with 4% paraformaldehyde for 15 min at room temperature with different time intervals after the illumination. Then they were permeabilized with 0.025% Triton X-100 in D-PBS (Sigma-Aldrich Corp., St. Louis, MO, USA) for 2 min. After washing with D-PBS three times, the cells were treated with 1% bovine serum albumin (BSA) for 2 h at 4°C. The fixed cells were stained with 5 nM Alexa Fluor® 488 phalloidin conjugate (Invitrogen, Eugene, OR, USA) for F-actin labeling for 40 min at 37°C. Meanwhile, 1% BSA was added to the staining solution to reduce nonspecific background staining. The cells were washed with 0.05% PBS-Tween20 three times before microscopic observation.

Microscopy and image analysis

The fluorescence images of cells were observed by a laser scanning confocal microscope (FV-300, IX71; Olympus, Tokyo, Japan) using a 488-nm continuous wave Ar⁺ laser (Melles Griot, Carlsbad, CA, USA) as the excitation source and a × 60 water objective to focus the laser beam. A 505- to 550-nm bandpass filter was used for the fluorescence images. Each experiment was repeated three times independently.

The fluorescence intensities of MMP, Ca²⁺, and NO probes from the microscopic images were analyzed with the Olympus Fluoview software. The data were expressed in terms of the relative fluorescence intensity of the probes and expressed as mean ± SD. The fluorescence intensity was averaged from 100 to 150 cells for each experiment.

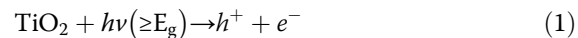
Results and discussion

Generation of ROS by pure and N-doped TiO₂ in aqueous suspensions

The generations of ROS induced by TiO₂ or N-TiO₂ nanoparticles in aqueous suspensions under visible light irradiation were studied using the fluorescence probes as described in the 'Methods' section. The fluorescence intensities with the irradiation times ranging from 1 to 5 min were shown in Figure 1a. The fluorescence intensities of both TiO₂ (the black line) and N-TiO₂ (the red line) samples increased with irradiation time but the fluorescence intensities of N-TiO₂ samples were always higher than that of the TiO₂ ones. It means that N-TiO₂ could generate more ROS than TiO₂ under visible light

irradiation, which agrees well with the spectral result that N-TiO₂ showed higher visible light absorption than TiO₂ (see Additional file 1: Figure S1, where a shoulder was observed at the edge of the absorption spectra, which extended the absorption of N-TiO₂ from 380 to 550 nm).

The major reactions for the formation of ROS upon illumination of TiO₂ have been proposed as follows [25]:



OH· is mainly formed in the reaction of photogenerated holes with surrounding water, while O₂^{·-} is formed in the reaction of photogenerated electrons with dissolved oxygen molecules. Some O₂^{·-} can form ¹O₂ by reacting with the holes. Moreover, some OH· can form H₂O₂, and the reactions of H₂O₂ can also result in the formation of OH· with a lesser extent.

Since DCFH is a nonspecific ROS probe, it is necessary to further analyze the specific ROS. As described above, DHR and APF were used to evaluate the generation of O₂^{·-}/H₂O₂ and OH·, respectively. The fluorescence measurements in Figure 1b,c shows that all the specific ROS increased with the irradiation time, but the N-TiO₂ induced more O₂^{·-}/H₂O₂ (Figure 1b) while less OH· (Figure 1c) than TiO₂. It was reported that the photogenerated holes of N-TiO₂ were trapped in the N 2p levels and had a very low mobility [26], thus were barely involved in the photocatalysis when the N-TiO₂ was illuminated by visible light [27]. In this study, the lower production of OH· from N-TiO₂ might result from the same reason. However, the photogenerated electrons in the conduction band can react with oxygen molecules to generate O₂^{·-}, which is thermodynamically favored [28]. Thus, N-TiO₂ could generate more O₂^{·-}/H₂O₂ than the pure TiO₂ due to the higher visible light absorption efficiency.

When cells were treated with TiO₂ or N-TiO₂ nanoparticles, the nanoparticles were not only found on the cell membrane but also in the cytoplasm, and some of them aggregated around or in Golgi complexes and even in nuclei [10]. As the TiO₂ or N-TiO₂ nanoparticles can induce ROS under visible light irradiation, the photokilling effect on cancer cells was observed in our previous work [10]. Considering that the productions of the specific ROS

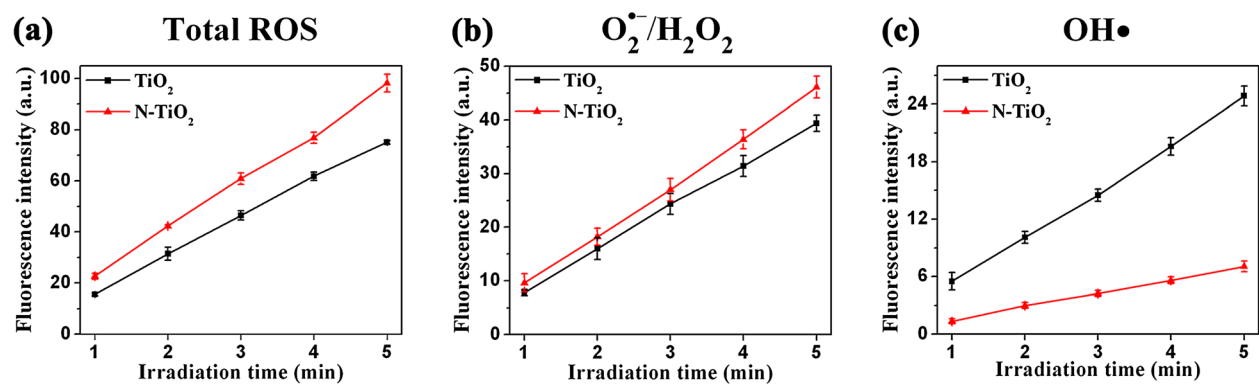


Figure 1 Comparison of ROS induced by TiO₂ and N-TiO₂. Fluorescence measurements as a function of irradiation time to compare the productions of ROS and specific ROS in aqueous suspensions induced by TiO₂ and N-TiO₂: (a) total ROS, (b) O₂⁻/H₂O₂, and (c) OH[•].

species generated by TiO₂ or N-TiO₂ are different and the contributions from the specific ROS to PDT may also be different, the PDT-induced changes of the intracellular parameters, such as MMP, Ca²⁺, and NO concentrations in HeLa cells treated with TiO₂ or N-TiO₂ were studied as follows.

MMP changes

When TiO₂- or N-TiO₂-treated cells were illuminated by light, the generated ROS may attack the mitochondria [29] or the activated nanoparticles may interact with the mitochondria directly [30], which would affect the function of mitochondria and cause the opening of mitochondrial permeability pores, resulting in the dissipation of MMP [30-32]. In this study, the MMP decreased immediately after the PDT as shown in Figure 2. It seems that the

mitochondrion is a very sensitive cellular organelle during the PDT, and the defects can be detected immediately in our study. For TiO₂-treated cells, the MMP level decreased continuously after the PDT with an approximate rate of 1.2% per min within 60 min. The MMP level for N-TiO₂ samples dropped much faster (around 4.2% per min) within the first 10 min after the PDT, then decreased at slower and slower rate within 45 min, and almost kept in a constant rate of 20% after 45 min. However, the MMP levels of control cells and the cells incubated with TiO₂ and N-TiO₂ under light-free conditions did not show any change during 60 min (data not shown), which confirmed the low cytotoxicity of TiO₂ and N-TiO₂.

It should be noted that the MMP level of N-TiO₂-treated cells decreased 3.5 times faster than that of the TiO₂-treated cells at the beginning after the PDT.

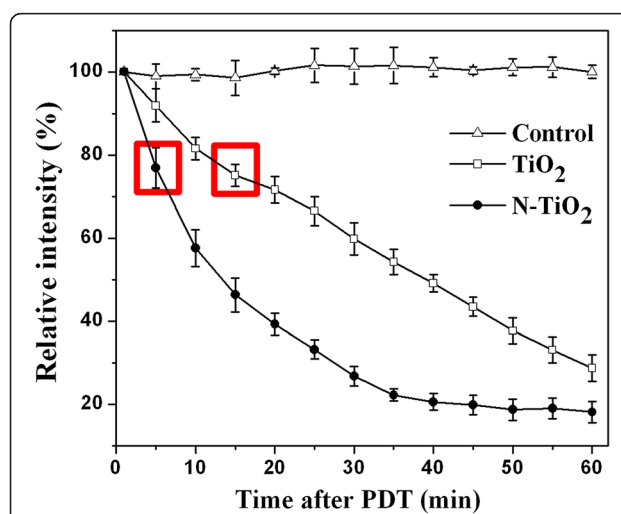


Figure 2 MMP of HeLa cells as a function of the time after the PDT. Cells were incubated with 100 µg/ml TiO₂ (white square) or N-TiO₂ (black circle) for 2 h and illuminated by the visible light for 5 min. The averaged fluorescence intensity of control cells (white triangle) at 0 min was set as 100%.

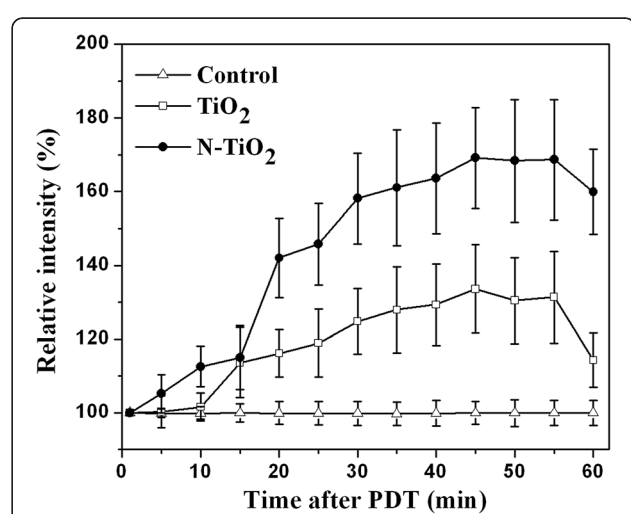


Figure 3 Time-dependent changes of the intracellular Ca²⁺ levels after the PDT. The averaged fluorescence intensity of control cells (white triangle) was set as 100%. TiO₂ (white square)- or N-TiO₂ (black circle)-treated cells (100 µg/ml) were incubated under light-free conditions for 2 h and illuminated by the visible light for 5 min.

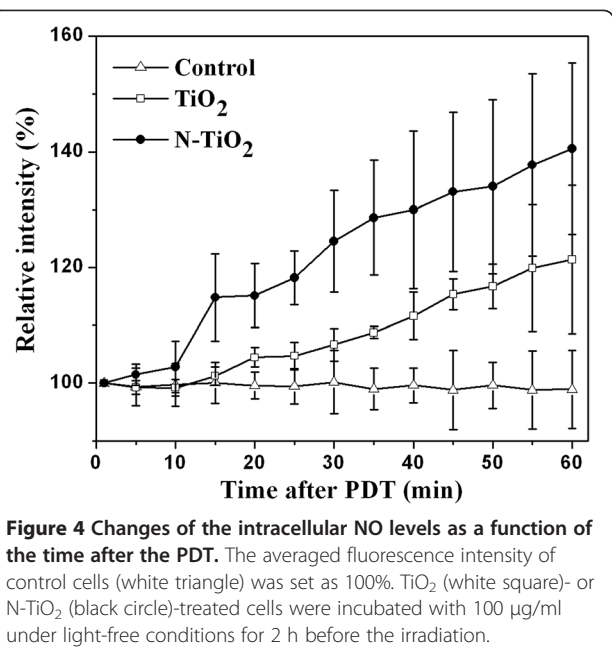


Figure 4 Changes of the intracellular NO levels as a function of the time after the PDT. The averaged fluorescence intensity of control cells (white triangle) was set as 100%. TiO₂ (white square)- or N-TiO₂ (black circle)-treated cells were incubated with 100 µg/ml under light-free conditions for 2 h before the irradiation.

Compared with Figure 1c that there were considerably more OH· induced by TiO₂ than N-TiO₂ under visible light, it strongly suggested that the hydroxyl radicals with the rather shorter lifetime and lower diffusion length than O₂⁻ and H₂O₂ [33] might contribute less on the damage of mitochondria among a variety of ROS in PDT.

Intracellular Ca²⁺ concentration

It has been reported that some signal transduction pathways were activated by PDT [34]. Calcium expression level was one of the concerning principal factor since it is an important link between the pathways. The

activation of Ca²⁺ was also known as a contributor to the cell morphological and functional changes associated with apoptosis [35]. The raise of intracellular calcium levels would result in various changes of cellular metabolism as well as the cell morphology.

The time-dependent intracellular Ca²⁺ concentrations after the PDT were measured as shown in Figure 3. The detectable increase of the intracellular Ca²⁺ levels for TiO₂ samples was first observed at 15 min after the PDT, while that for N-TiO₂ samples, it was observed at the first measurement point of 5 min after the PDT. Comparing the data in Figure 3 with that in Figure 2, we can see the elevation of Ca²⁺ followed by the loss of MMP. To demonstrate the correlativity of Ca²⁺ and MMP, the starting times of the detectable increase of Ca²⁺ were marked as two red squares in Figure 2. It suggests that a certain amount of the MMP loss (about 24% ± 5%) would cause the detectable increase of Ca²⁺.

As shown in Figure 3, the Ca²⁺ levels for both TiO₂ and N-TiO₂ samples reached the maximum values at about 45 min after the PDT, where N-TiO₂ induced release of Ca²⁺ at around 2.1-fold than TiO₂ did. Since there was no calcium ion in the D-PBS solution, the detected Ca²⁺ might be released from the damaged calcium stores, such as mitochondria and possibly other organelles, and flow into the cytoplasm through ion channels [36].

This result agreed with the data of MMP changes. The MMP levels of N-TiO₂ decreased around 3.5 times faster than that of TiO₂ at the early time after the PDT, which means the N-TiO₂ induced damage of mitochondria was more serious. Therefore, the released Ca²⁺ could be observed earlier and the Ca²⁺ levels were higher in N-TiO₂ samples as compared to the TiO₂ samples.

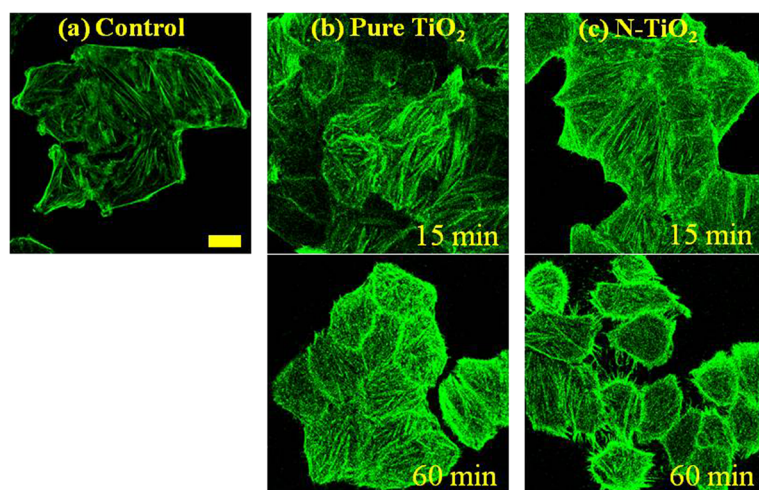


Figure 5 The morphology and cytoskeleton of HeLa cells at different time points after the PDT. (a) Control cells. (b) TiO₂-treated cells. (c) N-TiO₂-treated cells (scale bar, 20 µm). Cells were incubated with 100-µg/ml TiO₂ or N-TiO₂ under light-free conditions for 2 h before the PDT and then fixed at 15 min and 60 min after the PDT, respectively. The cells were stained with Alexa Fluor® 488 phalloidin for F-actin.

Generation of NO

The cells have defense mechanisms such as the endogenous generation of NO, which can scavenge a certain amount of ROS and protect cells from ROS attack [32,36,37]. The change of the NO level after the PDT was also detected in this work. The intracellular NO levels of N-TiO₂ samples increased faster than that of the TiO₂ ones (Figure 4), the former increased from 100% (as control cells) to 141% in 60 min after the PDT, while the latter increased to 121% only. It means that more NO was generated to buffer the increased ROS under higher oxidative stress for N-TiO₂ samples although TiO₂ induced higher amount of OH·. This result also suggested that the OH· species played a less important role among a variety of ROS in the PDT. Taken the above findings together, it suggested that the ROS overwhelmed the antioxidant defense capacity of NO in the cells, although NO could buffer the ROS to a certain extent. The remaining ROS would become highly harmful and lead to irreversible cellular damage.

Cell morphology and cytoskeleton defects

The cell morphology images of HeLa cells at different times after the PDT were acquired by a confocal microscope with the labeled F-actin. No morphology and cytoskeleton defects were found at 15 min after the PDT for both TiO₂ and N-TiO₂ samples (Figure 5b,c, upper images). At 60 min after the PDT, the organization of actin cytoskeleton of the cells incubated with TiO₂ seemed disrupted (Figure 5b, lower image), while the cells incubated with N-TiO₂ exhibited serious distortion and membrane breakage (Figure 5c, lower image).

As ROS can be generated around TiO₂ or N-TiO₂, the nanoparticles near the cell membranes may directly cause cell membrane damage by biochemical reactions. Additionally, the PDT-induced defect of mitochondria and the release of Ca²⁺ into the cytoplasm might trigger cell apoptosis or necrosis, which may result in the cell morphology and cytoskeleton defects eventually. As the cytoskeleton is involved in many intracellular signaling pathways, the cytoskeletal distortion and shrinkage need to be further studied for a long observation time in future studies.

Conclusions

A comparison of the killing effects between N-TiO₂ and TiO₂ on HeLa cells with visible light irradiation was conducted. N-TiO₂ produced more ROS and specifically more O₂·/H₂O₂ under visible light irradiation. Contrarily, more OH· were produced by TiO₂. The MMP levels were sensitive in the PDT, and rapid loss of MMP was detected at the very beginning after the PDT as one of the earliest detectable biochemical changes in this study. A certain amount of MMP loss (around 24%) was followed

by the detectable increase of Ca²⁺ (at 5 and 15 min after the PDT for N-TiO₂ and TiO₂, respectively). The increase of NO was detected later than the other intracellular parameters, which indicates that the NO generation was caused by the generation of ROS. The N-TiO₂ resulted in more loss of MMP and higher increase of Ca²⁺ and NO in HeLa cells and, finally, induced more cell damages than pure TiO₂. At 60 min after irradiation, significant cytoskeletal shrinkage and breakage were observed for N-TiO₂-treated cells, whereas for TiO₂-treated cells, only slight damage was demonstrated. Overall, N-TiO₂ can induce more cell damages than pure TiO₂. The hydroxyl radicals might contribute less to the cell damages among a variety of ROS.

Additional files

Additional file 1: Figure S1. Absorbance spectra of TiO₂ and N-TiO₂ nanoparticles. Description: A shoulder was observed at the edge of the absorption spectra, which extended the absorption of N-TiO₂ from 380 nm to 550 nm.

Additional file 2: Figure S2. The transmission spectrum of the 400 to 440 nm bandpass filter. Description: The filter could transmit some light with the wavelength below 400 nm, which could be absorbed by the pure TiO₂ as shown in Additional file 1: Figure S1.

Competing interests

The authors declare that they have no competing interests.

Authors' contributions

ZL carried out the experiments and drafted the manuscript. XP and TW participated in the confocal microscopy imaging. PW supervised the work, participated in the discussion of the results and in revising the manuscript. JC participated in the discussion of the results. LM designed the project and wrote the manuscript. All authors read and approved the final manuscript.

Acknowledgments

This work is supported by the National Natural Science Foundation of China (61008055, 11074053), the Ph.D. Programs Foundation of Ministry of Education of China (20100071120029), and the Key Subjects Innovative Talents Training Program of Fudan University.

Author details

¹Key Laboratory of Micro and Nano Photonic Structures (Ministry of Education), Department of Optical Science and Engineering, Shanghai Ultra-Precision Optical Manufacturing Engineering Center, Fudan University, 220 Handan Road, Shanghai 200433, China. ²State Key Laboratory of Surface Physics, Department of Physics, Fudan University, 220 Handan Road, Shanghai 200433, China.

Received: 14 December 2012 Accepted: 29 January 2013

Published: 22 February 2013

References

1. Cai R, Hashimoto K, Itoh K, Kubota Y, Fujishima A: Photokilling of malignant-cells with ultrafine TiO₂ powder. *B Chem Soc Jpn* 1991, 64:1268–1273.
2. Cai R, Kubota Y, Shuin T, Sakai H, Hashimoto K, Fujishima A: Induction of cytotoxicity by photoexcited TiO₂ particles. *Cancer Res* 1992, 52:2346–2348.
3. Wamer WG, Yin JJ, Wei RR: Oxidative damage to nucleic acids photosensitized by titanium dioxide. *Free Radical Biol Med* 1997, 23:851–858.
4. Rozhkova EA, Ulasov I, Lai B, Dimitrijevic NM, Lesniak MS, Rajh T: A high-performance nanobio photocatalyst for targeted brain cancer therapy. *Nano Lett* 2009, 9:3337–3342.

5. Nosaka Y, Nakamura M, Hirakawa T: Behavior of superoxide radicals formed on TiO_2 powder photocatalysts studied by a chemiluminescent probe method. *Phys Chem Chem Phys* 2002, **4**:1088–1092.
6. Murakami Y, Kenji E, Nosaka AY, Nosaka Y: Direct detection of OH radicals diffused to the gas phase from the UV-irradiated photocatalytic TiO_2 surfaces by means of laser-induced fluorescence spectroscopy. *J Phys Chem B* 2006, **110**:16808–16811.
7. Janczyk A, Krakowska E, Stochel G, Macyk W: Singlet oxygen photogeneration at surface modified titanium dioxide. *J Am Chem Soc* 2006, **128**:15574–15575.
8. Kubo W, Tatsuma T: Detection of H_2O_2 released from TiO_2 photocatalyst to air. *Anal Sci* 2004, **20**:591–593.
9. Lagopati N, Kitsiou PV, Kontos AI, Venieratos P, Kotsopoulos E, Kontos AG, Dionysiou DD, Pispas S, Tsilibary EC, Falaras P: Photo-induced treatment of breast epithelial cancer cells using nanostructured titanium dioxide solution. *J Photoch Photobio A* 2010, **214**:215–223.
10. Li Z, Mi L, Wang PN, Chen JY: Study on the visible-light-induced photokilling effect of nitrogen-doped TiO_2 nanoparticles on cancer cells. *Nanoscale Res Lett* 2011, **6**:356.
11. Chen X, Mao SS: Titanium dioxide nanomaterials: synthesis, properties, modifications, and applications. *Chem Rev* 2007, **107**:2891–2959.
12. Janczyk A, Wolnicka-Glibisz A, Urbanska K, Stochel G, Macyk W: Photocytotoxicity of platinum(IV)-chloride surface modified TiO_2 irradiated with visible light against murine macrophages. *J Photoch Photobio B* 2008, **92**:54–58.
13. Janczyk A, Wolnicka-Glibisz A, Urbanska K, Kisch H, Stochel G, Macyk W: Photodynamic activity of platinum (IV) chloride surface-modified TiO_2 irradiated with visible light. *Free Radical Bio Med* 2008, **44**:1120–1130.
14. Huang KQ, Chen L, Xiong JW, Liao MX: Preparation and characterization of visible-light-activated Fe-N Co-doped TiO_2 and its photocatalytic inactivation effect on leukemia tumors. *Int J Photoenergy* 2012, **2012**:9.
15. Xu SJ, Shen JQ, Chen S, Zhang MH, Shen T: Active oxygen species (${}^1\text{O}_2$, O_2^-) generation in the system of TiO_2 colloid sensitized by hypocrellin B. *J Photoch Photobio B* 2002, **67**:64–70.
16. Tokuoka Y, Yamada M, Kawashima N, Miyasaka T: Anticancer effect of dye-sensitized TiO_2 nanocrystals by polychromatic visible light irradiation. *Chem Lett* 2006, **35**:496–497.
17. Tsai T, Ji HT, Chiang PC, Chou RH, Chang WSW, Chen CT: ALA-PDT results in phenotypic changes and decreased cellular invasion in surviving cancer cells. *Laser Surg Med* 2009, **41**:305–315.
18. Tapajos ECC, Longo JP, Simioni AR, Lacava ZGM, Santos MFMA, Morais PC, Tedesco AC, Azevedo RB: In vitro photodynamic therapy on human oral keratinocytes using chloroaluminum-phthalocyanine. *Oral Oncol* 2008, **44**:1073–1079.
19. Xiao L, Gu L, Howell SB, Sailor MJ: Porous silicon nanoparticle photosensitizers for singlet oxygen and their phototoxicity against cancer cells. *ACS Nano* 2011, **5**:3651–3659.
20. Bhattacharya S, Kudgus RA, Bhattacharya R, Mukherjee P: Inorganic nanoparticles in cancer therapy. *Pharm Res-Dordr* 2011, **28**:237–259.
21. Cathcart R, Schwiers E, Ames BN: Detection of picomole levels of hydroperoxides using a fluorescent dichlorofluorescein assay. *Anal Biochem* 1983, **134**:111–116.
22. Bueb JL, Gallois A, Schneider JC, Parini JP, Tschirhart E: A double-labeling fluorescent assay for concomitant measurements of $[\text{Ca}^{2+}]_i$ and O_2^- production in human macrophages. *Bba-Gen Subjects* 1995, **1244**:79–84.
23. Freitas M, Lima JLFC, Fernandes E: Optical probes for detection and quantification of neutrophils' oxidative burst. A review. *Anal Chim Acta* 2009, **649**:8–23.
24. Gomes A, Fernandes E, Lima JL: Fluorescence probes used for detection of reactive oxygen species. *J Biomed Bioph Meth* 2005, **65**:45–80.
25. Bahirini C, Parker A, Schoemaecker C, Fittschen C: Direct detection of HO_2 radicals in the vicinity of TiO_2 photocatalytic surfaces using cw-CRDS. *Appl Catal B-Environ* 2010, **99**:413–419.
26. Tafen DN, Wang J, Wu NQ, Lewis JP: Visible light photocatalytic activity in nitrogen-doped TiO_2 nanobelts. *Appl Phys Lett* 2009, **94**:093101.
27. Wang J, Tafen DN, Lewis JP, Hong ZL, Manivannan A, Zhi MJ, Li M, Wu NQ: Origin of photocatalytic activity of nitrogen-doped TiO_2 nanobelts. *J Am Chem Soc* 2009, **131**:12290–12297.
28. Fujishima A, Rao TN, Tryk DA: Titanium dioxide photocatalysis. *J Photoch Photobio C* 2000, **1**:1–21.
29. Tian YY, Xu DD, Tian X, Cui FA, Yuan HQ, Leung WN: Mitochondria-involved apoptosis induced by MPPa mediated photodynamic therapy. *Laser Phys Lett* 2008, **5**:746–751.
30. Soto K, Garza KM, Murr LE: Cytotoxic effects of aggregated nanomaterials. *Acta Biomater* 2007, **3**:351–358.
31. Vaseva AV, Marchenko ND, Ji K, Tsirka SE, Holzmann S, Moll UM: p53 opens the mitochondrial permeability transition pore to trigger necrosis. *Cell* 2012, **149**:1536–1548.
32. Simon HU, Haj-Yehia A, Levi-Schaffer F: Role of reactive oxygen species (ROS) in apoptosis induction. *Apoptosis* 2000, **5**:415–418.
33. Dimitrijevic NM, Rozhkova E, Rajh T: Dynamics of localized charges in dopamine-modified TiO_2 and their effect on the formation of reactive oxygen species. *J Am Chem Soc* 2009, **131**:2893–2899.
34. Robertson CA, Evans DH, Abrahamse H: Photodynamic therapy (PDT): a short review on cellular mechanisms and cancer research applications for PDT. *J Photoch Photobio B* 2009, **96**:1–8.
35. Hui HX, Dotta F, Di Mario U, Perfetti R: Role of caspases in the regulation of apoptotic pancreatic islet beta-cells death. *J Cell Physiol* 2004, **200**:177–200.
36. Almeida RD, Manadas BJ, Carvalho AP, Duarte CB: Intracellular signaling mechanisms in photodynamic therapy. *Biochim Biophys Acta* 2004, **1704**:59–86.
37. Gomes ER, Almeida RD, Carvalho AP, Duarte CB: Nitric oxide modulates tumor cell death induced by photodynamic therapy through a cGMP-dependent mechanism. *Photochem Photobiol* 2002, **76**:423–430.

doi:10.1186/1556-276X-8-96

Cite this article as: Li et al.: Comparison of the killing effects between nitrogen-doped and pure TiO_2 on HeLa cells with visible light irradiation. *Nanoscale Research Letters* 2013 **8**:96.

Submit your manuscript to a SpringerOpen® journal and benefit from:

- Convenient online submission
- Rigorous peer review
- Immediate publication on acceptance
- Open access: articles freely available online
- High visibility within the field
- Retaining the copyright to your article

Submit your next manuscript at ► springeropen.com